# Antibonding Induced Anharmonicity Leading to Ultralow Lattice Thermal Conductivity and Extraordinary Thermoelectric Performance in CsK$_2$X (X = Sb, Bi)

Kunpeng Yuan[1], Xiaoliang Zhang[1*], Zheng Chang[1], Dawei Tang[1*], and Ming Hu[2*]

[1]*Key Laboratory of Ocean Energy Utilization and Energy Conservation of Ministry of Education, School of Energy and Power Engineering, Dalian University of Technology, Dalian 116024, China.*
[2]*Department of Mechanical Engineering, University of South Carolina, Columbia, 29208, USA*

*Corresponding author. zhangxiaoliang@dlut.edu.cn (X.Z.); dwtang@dlut.edu.cn (D.T.); hu@sc.edu (M.H.)*

# 1. Test of moment tensor potential (MTP)

To test the accuracy of our MTP model, we performed extra classical MD with the LAMMPS package[1] and MTP model in the temperature range from 100 to 800 K with the interval of 100 K, and extracted 80 random configurations as validation data sets. The energies and interatomic forces of these random configurations were further calculated from DFT and then compared with the MTP results. The maximum and average absolute errors of MTP for the training and validation sets are shown in Table S1.

**Table S1**. The maximum and average absolute errors of MTP for the training and validation sets.

| Materials | Data sets | Energy per atom (meV) | | Force (meV/Å) | |
|---|---|---|---|---|---|
| | | Maximum | Average | Maximum | Average |
| $CsK_2Sb$ | Training | 3.369 | 0.149 | 303.4 | 3.145 |
| | Validation | 3.686 | 0.125 | 289.8 | 2.825 |
| $CsK_2Bi$ | Training | 3.175 | 0.124 | 287.2 | 3.308 |
| | Validation | 3.238 | 0.122 | 247.0 | 3.338 |

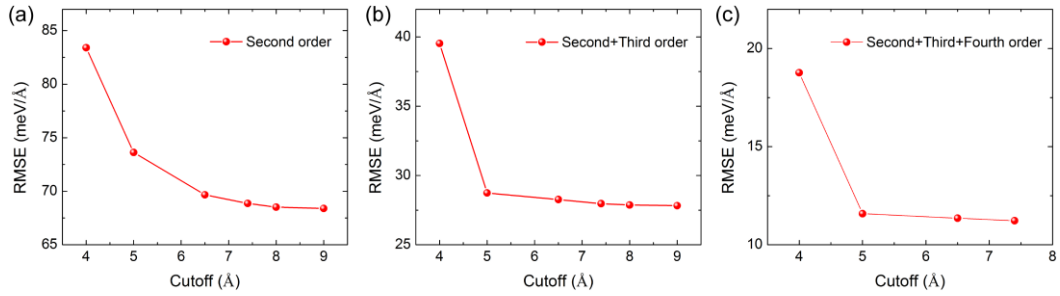# 2. Convergence test for interatomic force constants



**Figure S1.** Root mean square errors (RMSE) of atomic force with respect to the cutoff distances for the (a) second-, (b) third-, and (c) fourth-order force constants of $CsK_2Sb$.
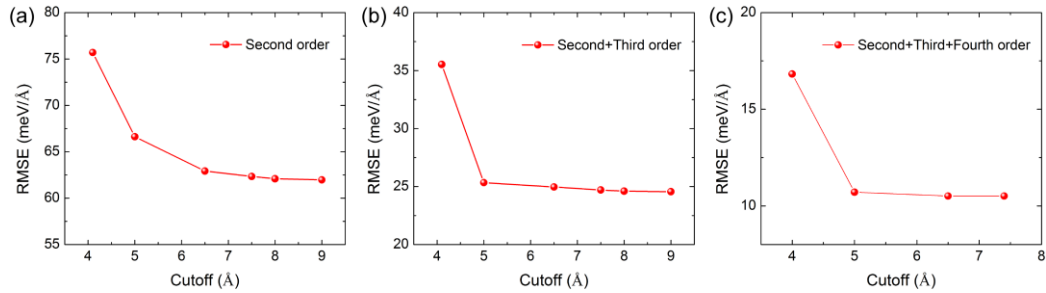


**Figure S2.** Root mean square errors (RMSE) of atomic force with respect to the cutoff distances for the (a) second-, (b) third-, and (c) fourth-order force constants of $CsK_2Bi$.

## 3. Different mechanisms of carrier scattering

In the calculations of carrier scattering rates, the acoustic deformation potential scattering (AD), polar optical phonon scattering (PO), and ionized impurities (IM) are considered.[2]

The acoustic deformation potential scattering (AD) relies on the deformation potentials and elastic constants, and the scattering matrix is given by

$$g_{im}^{AD}(\mathbf{k},\mathbf{q}) = \sqrt{k_B T} \sum_{\mathbf{G} \neq \mathbf{q}} \left[ \frac{\tilde{\mathbf{D}}_{i\mathbf{k}} : \tilde{\mathbf{S}}_l}{c_l \sqrt{\rho}} + \frac{\tilde{\mathbf{D}}_{i\mathbf{k}} : \tilde{\mathbf{S}}_{t_1}}{c_{t_1} \sqrt{\rho}} + \frac{\tilde{\mathbf{D}}_{i\mathbf{k}} : \tilde{\mathbf{S}}_{t_2}}{c_{t_2} \sqrt{\rho}} \right] <m\mathbf{k}+\mathbf{q}\,|\,e^{i(\mathbf{q}+\mathbf{G})\cdot\mathbf{r}}\,|\,i\mathbf{k}> \quad (1)$$

where $\tilde{\mathbf{D}}_{i\mathbf{k}} = \mathbf{D}_{i\mathbf{k}} + \mathbf{v}_{i\mathbf{k}} \otimes \mathbf{v}_{i\mathbf{k}}$ in which $\mathbf{D}_{i\mathbf{k}}$ is the second rank deformation potential tensor and $\mathbf{v}_{i\mathbf{k}}$ is the group velocity, $\hat{\mathbf{S}} = \mathbf{q} \otimes \mathbf{u}$ is the unit strain associated with an acoustic mode, $\mathbf{u}$ is the unit vector of phonon polarization, $\rho$ is the density, $c$ is the phonon group velocity, and the subscripts $l$, $t_1$, and $t_2$ indicate properties belonging to the longitudinal and transverse modes.

$$g_{im}^{AD}(\mathbf{k},\mathbf{q}) = \left( \frac{k_B T \varepsilon_d^2}{B} \right)^{1/2} <\psi_{\mathbf{k}+\mathbf{q}}\,|\,\psi_{\mathbf{k}}> \quad (2)$$

The polar optical phonon scattering matrix is written as

$$g_{im}^{PO}(\mathbf{k},\mathbf{q}) = \left[ \frac{\hbar \omega_{po}}{2} \right]^{1/2} \sum_{\mathbf{G} \neq \mathbf{q}} \left( \frac{1}{\hat{\mathbf{n}} \cdot \boldsymbol{\varepsilon}_\infty \cdot \hat{\mathbf{n}}} - \frac{1}{\hat{\mathbf{n}} \cdot \boldsymbol{\varepsilon}_s \cdot \hat{\mathbf{n}}} \right)^{1/2}$$
$$\times \frac{<m\mathbf{k}+\mathbf{q}\,|\,e^{i(\mathbf{q}+\mathbf{G})\cdot\mathbf{r}}\,|\,i\mathbf{k}>}{|\mathbf{q}+\mathbf{G}|} \quad (3)$$

where $\boldsymbol{\varepsilon}_s$ and $\boldsymbol{\varepsilon}_\infty$ are the static and high-frequency dielectric tensors and $\omega_{po}$ is the polar optical phonon frequency, $\hat{\mathbf{n}}$ is the unit vector in the direction of scattering.

$$g_{im}^{PO}(\mathbf{k},\mathbf{q}) = \left[ \frac{\hbar \omega_{po}}{2} \left( \frac{1}{\varepsilon_\infty} - \frac{1}{\varepsilon_s} \right) \right]^{1/2} \frac{<\psi_{\mathbf{k}+\mathbf{q}}\,|\,\psi_{\mathbf{k}}>}{|\mathbf{q}|} \quad (4)$$

The ionized impurity matrix element is given by

$$g_{im}^{IM}(\mathbf{k},\mathbf{q}) = \sum_{\mathbf{G} \neq \mathbf{q}} \frac{n_{ii}^2 Z e}{\hat{\mathbf{n}} \cdot \boldsymbol{\varepsilon}_s \cdot \hat{\mathbf{n}}} \frac{<m\mathbf{k}+\mathbf{q}\,|\,e^{i(\mathbf{q}+\mathbf{G})\cdot\mathbf{r}}\,|\,i\mathbf{k}>}{|\mathbf{q}+\mathbf{G}|^2 + \beta^2} \quad (5)$$

where $Z$ is the charge state of the impurity center, $e$ is the electron charge, $n_{ii} = (n_h -$

$n_e)/Z$ is the concentration of ionized impurities, and $\beta$ is the inverse screening length. The above parameters are prepared by first-principles calculations.
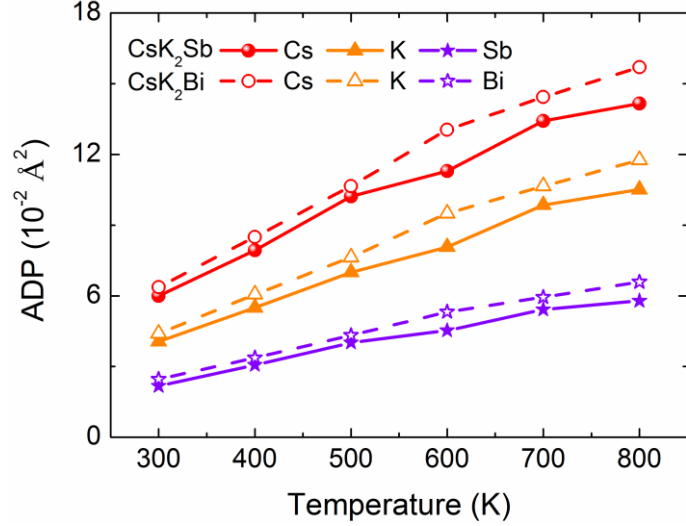
## 4. Atomic displacement parameters



**Figure S3.** Calculated temperature-dependent isotropic atomic displacement parameters (ADP) of each inequivalent atom of $CsK_2Sb$ and $CsK_2Bi$.
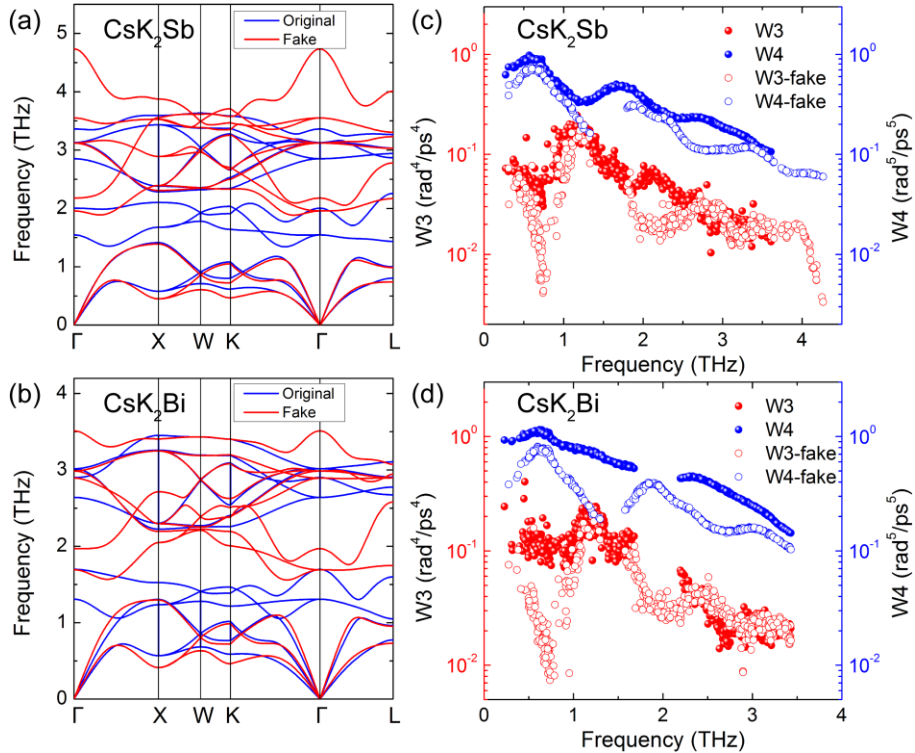
## 5. Weighted scattering phase space of $CsK_2Sb$ and $CsK_2Bi$



**Figure S4.** Comparison of original and fake phonon dispersion of (a) $CsK_2Sb$ and (b) $CsK_2Bi$. The fake phonon dispersion is obtained by artificially reducing the atomic mass of Sb/Bi by a factor of three. (c-d) Weighted three- and four-phonon scattering phase space based on the original and reduced atomic mass of Sb/Bi.
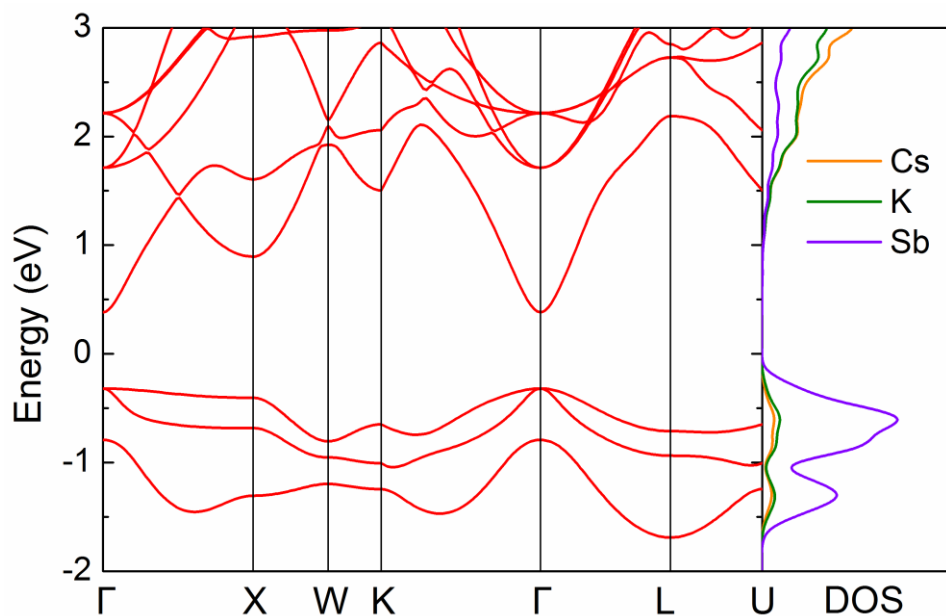
## 6. Band structures of CsK₂Sb and CsK₂Bi



**Figure S5.** Band structure and atom projected density of states (DOS) of CsK$_2$Sb based on PBE exchange functional including SOC.
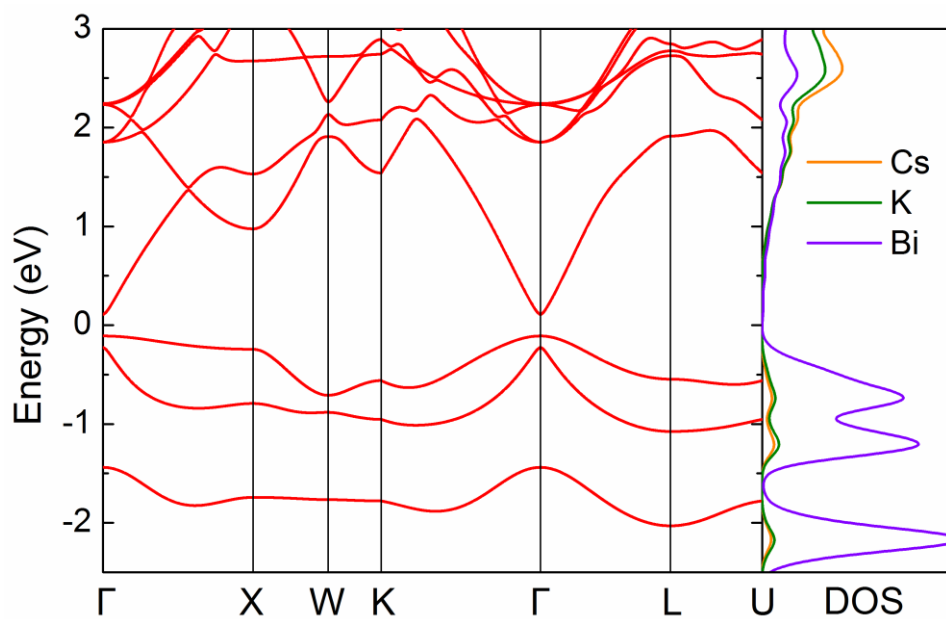


**Figure S6.** Band structure and atom projected density of states (DOS) of CsK$_2$Bi based on PBE exchange functional including SOC. The band gap is corrected by the HSE06 functional.
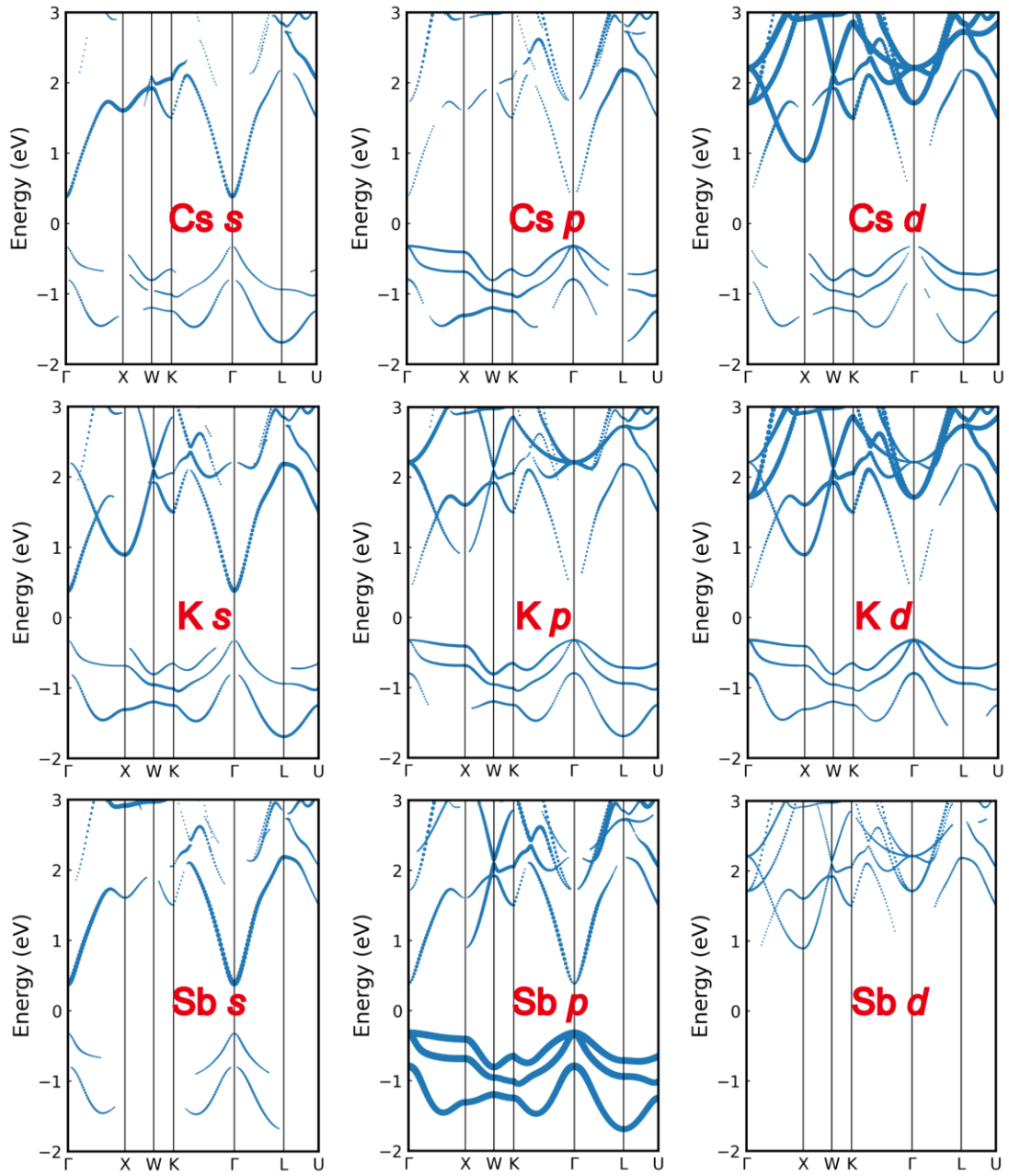
**Figure S7.** Orbital-projected band structures of CsK$_2$Sb. The size of the band is proportional to the relative contribution of the highlighted orbital to the bands.

**Figure S8.** Orbital-projected band structures of CsK$_2$Bi. The size of the band is proportional to the relative contribution of the highlighted orbital to the bands.
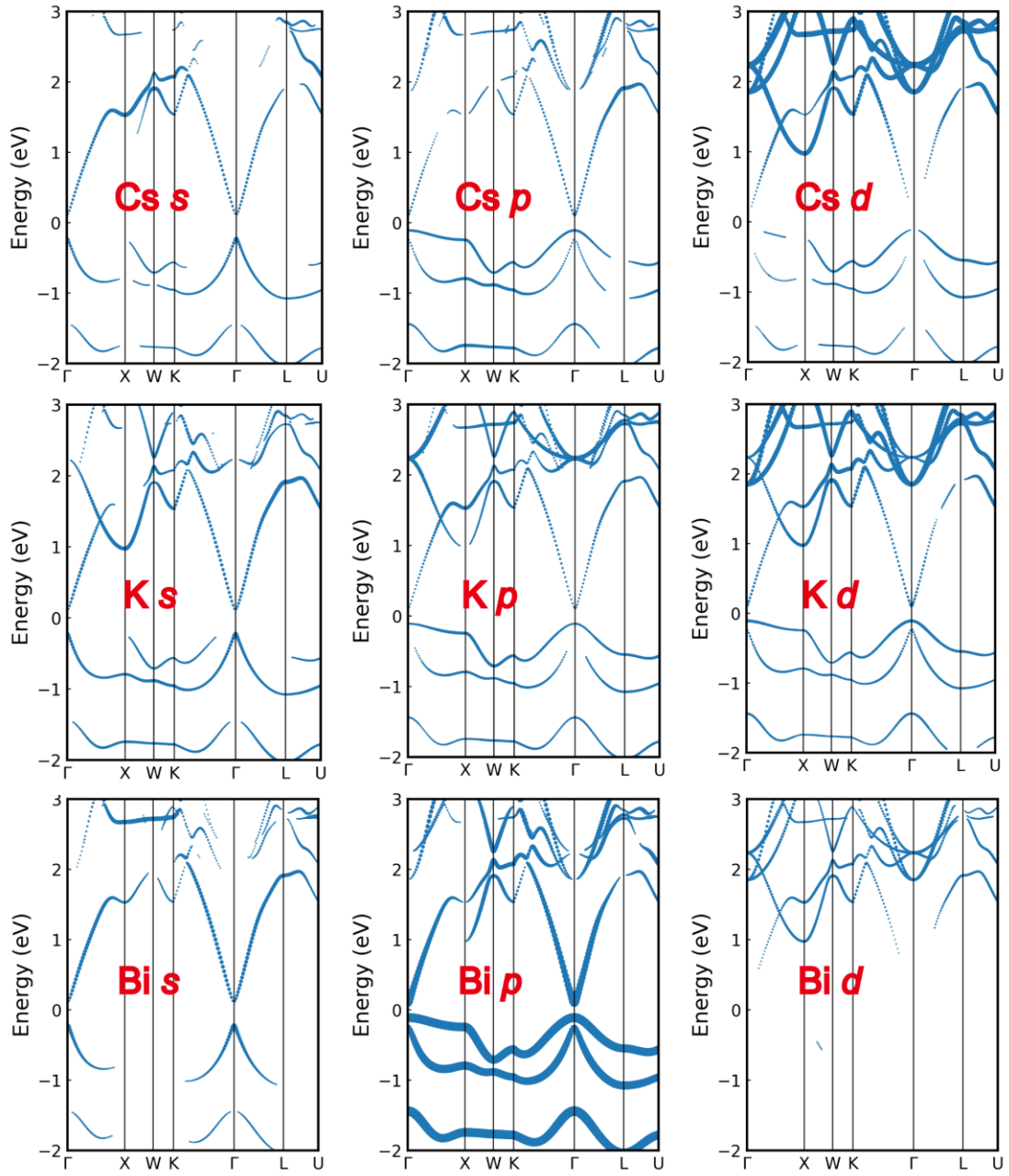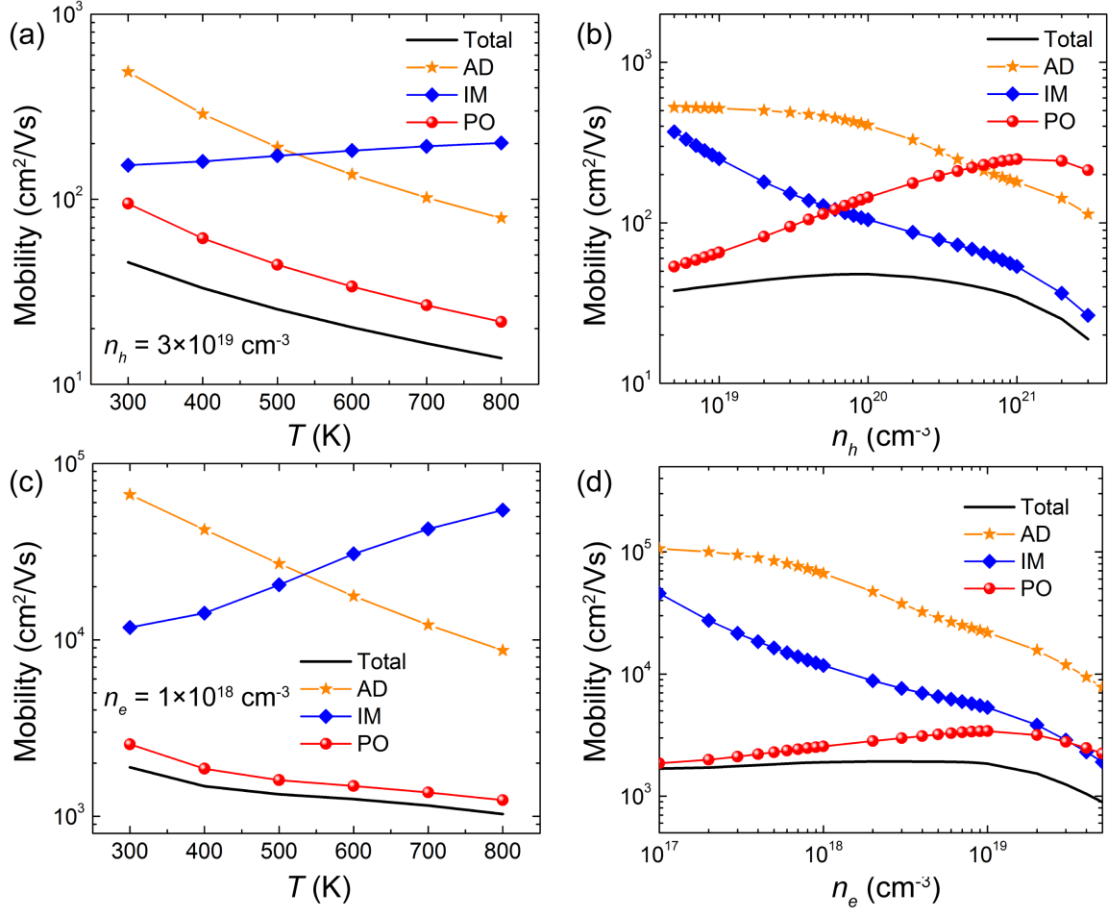
## 7. Carrier mobility of CsK$_2$Bi



**Figure S9.** (a) Hole mobility of CsK$_2$Bi at a hole concentration of $3 \times 10^{19}$ cm$^{-3}$ as a function of temperature. (b) Room-temperature hole mobility of CsK$_2$Bi against hole concentration. (c) Electron mobility of CsK$_2$Bi at an electron concentration of $1 \times 10^{18}$ cm$^{-3}$ as a function of temperature. (d) Room-temperature electron mobility of CsK$_2$Bi against electron concentration. AD, IM, and PO represent the acoustic deformation potential scattering, ionized impurity scattering, and polar optical phonon scattering.

## 8. Electronic transport properties of CsK$_2$Bi

As shown in Figure S10, due to the small band gap, CsK$_2$Bi exhibits a few distinct electronic transport properties compared to CsK$_2$Sb. At 800 K, the absolute value of Seebeck coefficient in the range of low carrier concentration is much lower than that at 300 K. It should also be noted that there is a sign reverse of the Seebeck coefficient in Figure S10(a), implying that the thermoelectric properties change from the *p*-type to *n*-type at very low levels of *p*-type doping. Opposite to the Seebeck coefficient, the electrical conductivity is higher at 800 K in the range of low carrier concentration. These behaviors are clear indications of the strong bipolar effect, which is usually

significant in semiconductors with a narrow band gap (< 0.5 eV).[3] This effect occurs when electrons are thermally excited across the band gap producing minority charge carriers (e.g. electrons in a *p*-type material or holes in an *n*-type material). Moreover, the bipolar effect should be remarkable in a material with low external dopant concentration since the thermally excited carriers will have a higher proportion compared to the external doped carriers. As a consequence, the electrical conductivity and electronic thermal conductivity will benefit from the bipolar effect due to the dual contribution of different types of carriers. However, the bipolar effect will suppress the Seebeck coefficient since the contributions from the two types of carriers have opposite signs.

The maximum room-temperature power factor for *p*-type $CsK_2Bi$ can reach 4.5 mW/mK$^2$, while the *n*-type counterpart is 1.3. The power factor of $CsK_2Bi$ is slightly larger than that of $CsK_2Sb$ due to the higher electrical conductivity. However, owing to the dominant role of electronic thermal conductivity at high carrier concentration, the maximum *ZT* will be achieved in a lower carrier concentration compared to the power factor.
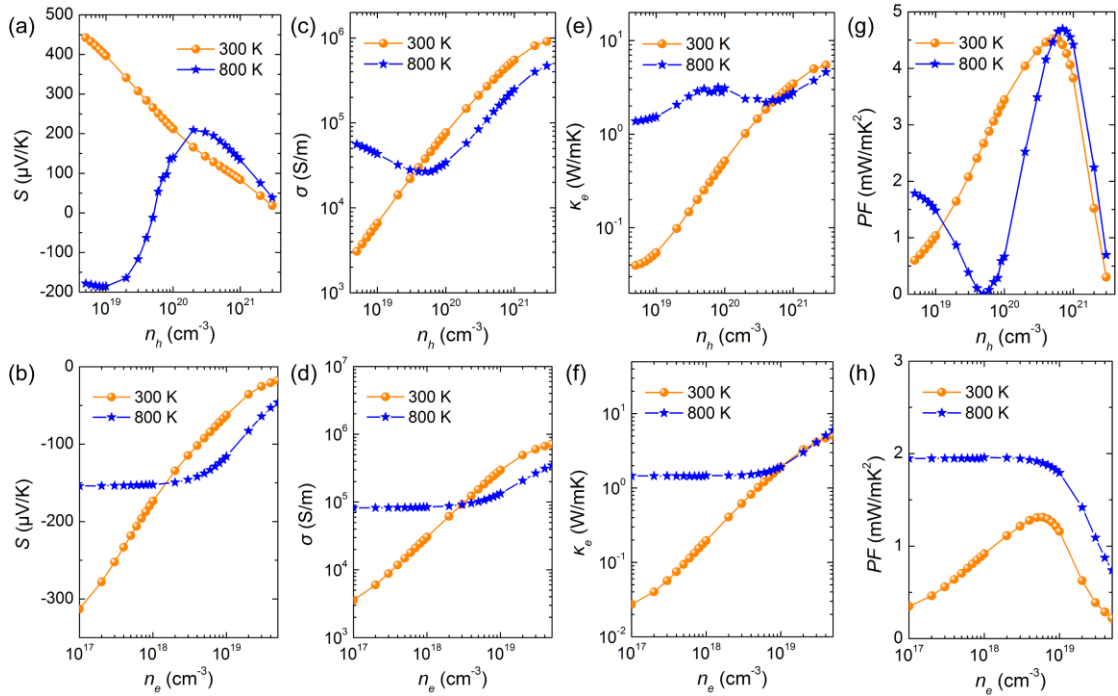


**Figure S10.** Electronic transport properties of $CsK_2Bi$. (a, b) Seebeck coefficient, (c, d) electrical conductivity, (e, f) electronic thermal conductivity, and (g, h) power factor as a function of hole and electron concentration.
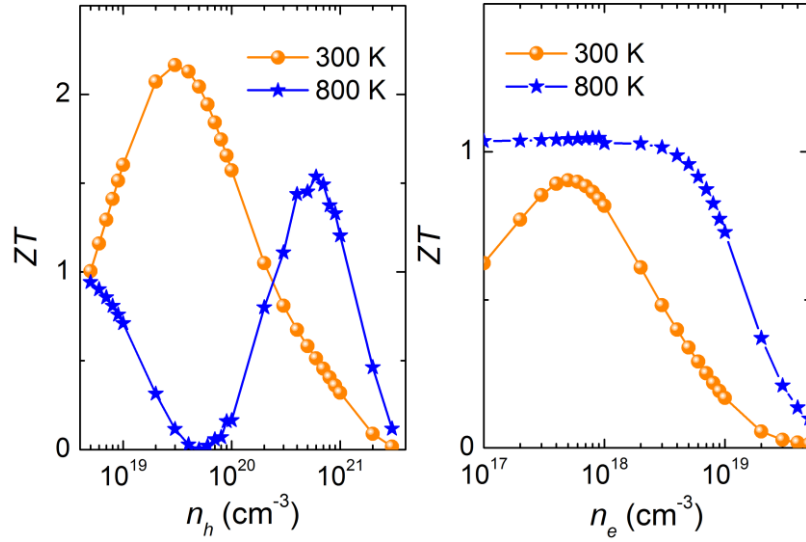
**Figure S11.** Calculated figure of merit of CsK$_2$Bi as a function of hole and electron concentration.

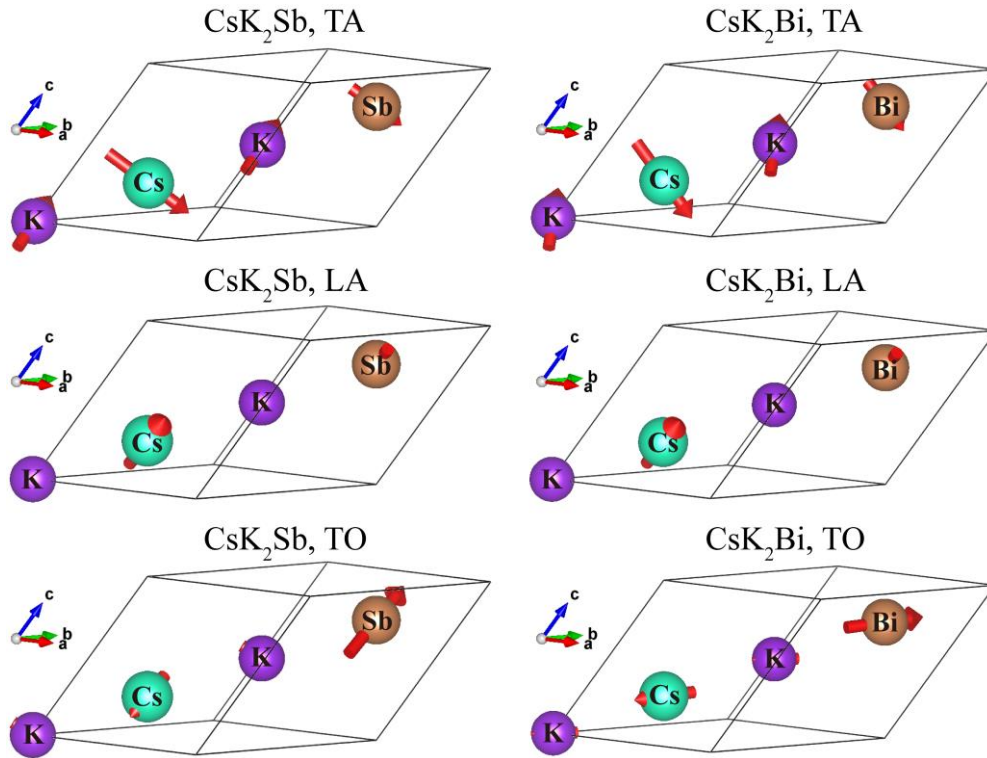## 9. Atomic collective vibration vectors



**Figure S12.** Atomic collective vibration vectors for the representative TA, LA, and TO phonon modes at the (0.5, 0.0, 0.5) point in the reciprocal space for CsK$_2$Sb and CsK$_2$Bi.

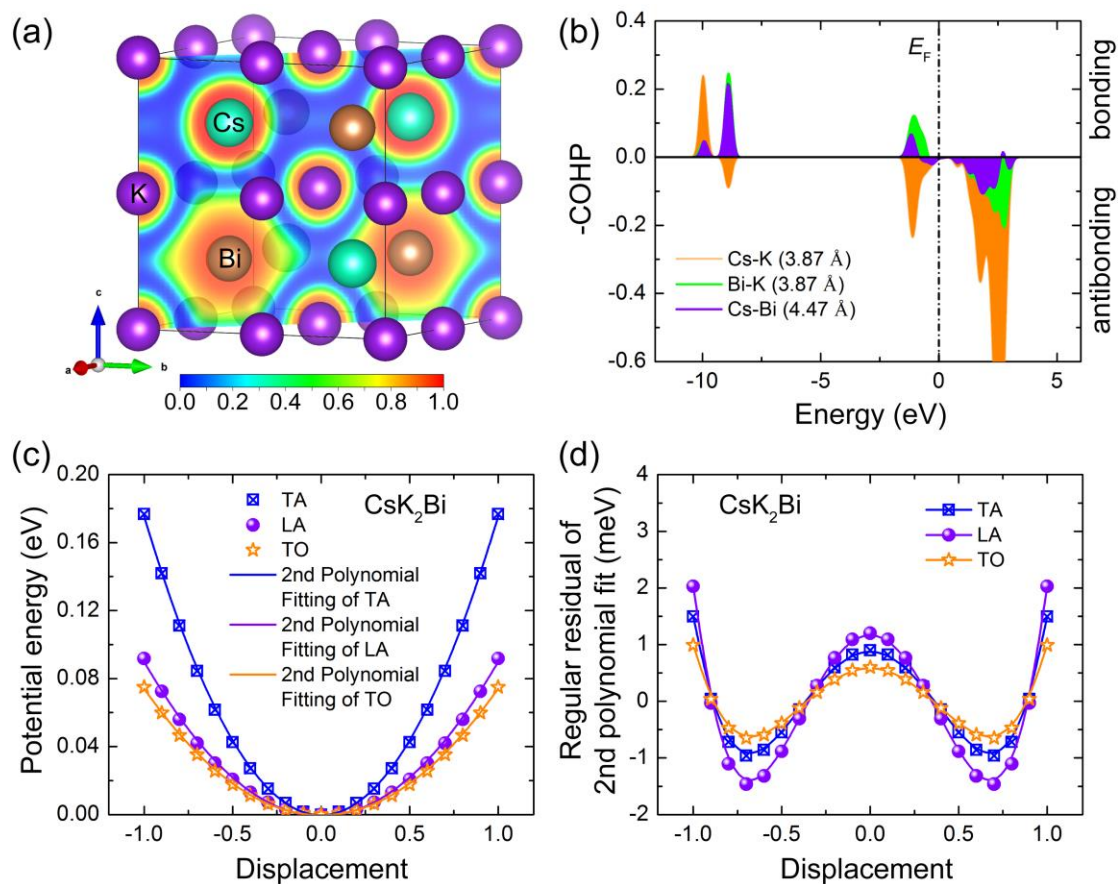## 10. Bonding nature and regular residual analysis of CsK₂Bi



**Figure S13.** (a) Electron localization function of CsK₂Bi along the (110) plane of the conventional cell. (b) COHP projected on Cs-K, Bi-K, and Cs-Bi bonds. The bond length is included in the parenthesis. (c) Potential energy variation as a function of displacement for representative phonon modes of CsK₂Bi. (d) Regular residual analysis of the second polynomial fit to the potential energy curves.

## References

1.    Plimpton, S., Fast parallel algorithms for short-range molecular dynamics. *Journal of Computational Physics* 1995, 117, 1-19.

2.    Ganose, A. M.; Park, J.; Faghaninia, A.; Woods-Robinson, R.; Persson, K. A.; Jain, A., Efficient calculation of carrier scattering rates from first principles. *Nature communications* 2021, 12, 2222.

3.    Gong, J. J.; Hong, A. J.; Shuai, J.; Li, L.; Yan, Z. B.; Ren, Z. F.; Liu, J. M., Investigation of the bipolar effect in the thermoelectric material CaMg₂Bi₂ using a first-principles study. *Physical Chemistry Chemical Physics* 2016, 18, 16566-16574.